LETTERS
PUBLISHED ONLINE: 21 NOVEMBER 2016 | DOI: 10.1038/NNANO.2016.241
nature nanotechnology

Probing the electronic and catalytic properties of a bimetallic surface with 3 nm resolution

Jin-Hui Zhong[1†], Xi Jin[1†], Lingyan Meng[2], Xiang Wang[1], Hai-Sheng Su[1], Zhi-Lin Yang[2], Christopher T. Williams[3] and Bin Ren[1*]

An atomic- and molecular-level understanding of heterogeneous catalysis is required to characterize the nature of active sites and improve the rational design of catalysts[1–3]. Achieving this level of characterization requires techniques that can correlate catalytic performances to specific surface structures, so as to avoid averaging effects[1]. Tip-enhanced Raman spectroscopy[4–7] combines scanning probe microscopy with plasmon-enhanced Raman scattering and provides simultaneous topographical and chemical information at the nano/atomic scale from ambient[8–10] to ultrahigh-vacuum[11,12] and electrochemical environments[13,14]. Therefore, it has been used to monitor catalytic reactions[15–18] and is proposed to correlate the local structure and function of heterogeneous catalysts[19]. Bimetallic catalysts, such as Pd–Au, show superior performance in various catalytic reactions[20,21], but it has remained challenging to correlate structure and reactivity because of their structural complexity. Here, we show that TERS can chemically and spatially probe the site-specific chemical (electronic and catalytic) and physical (plasmonic) properties of an atomically well-defined Pd(sub-monolayer)/Au(111) bimetallic model catalyst at 3 nm resolution in real space using phenyl isocyanide as a probe molecule (Fig. 1a). We observe a weakened N≡C bond and enhanced reactivity of phenyl isocyanide adsorbed at the Pd step edge compared with that at the Pd terrace. Density functional theory corroborates these observations by revealing a higher *d*-band electronic profile for the low-coordinated Pd step edge atoms. The 3 nm spatial resolution we demonstrate here is the result of an enhanced electric field and distinct electronic properties at the step edges.

We prepared a well-defined bimetallic model catalyst by electrochemical underpotential deposition of a monoatomic Pd layer with different coverages on a well-ordered Au(111) single-crystal surface (Fig. 1b). ML denotes the full monolayer and 0.8 ML indicates 0.8 coverage. Scanning tunnelling microscopy (STM) images of the bare Au(111) (Fig. 1c) and Pd_{ML}/Au(111) (Fig. 1e) substrates show continuous atomic flat surfaces, and that of the $Pd_{0.8ML}$/Au(111) sample (Fig. 1d) shows some Au holes in the continuous Pd monoatomic layer. Therefore, it contains not only Pd and Au surface sites, but also Pd–Au interfacial sites, representing a typical state-of-the-art bimetallic catalyst surface. These atomically well-defined bimetallic surfaces allow a clear structure–function relationship to be explored at atomic and molecular levels.

Phenyl isocyanide (PIC) (Fig. 2b, inset)[22] was then used as a Raman probe to detect the electronic and catalytic properties of the surface. The N≡C stretching frequency (ν_{NC}) of PIC is sensitive to the atomic geometry and electronic structure of metal surfaces[23,24]. Compared with a bare Au(111) surface (Fig. 1c), some single atomic layer vacancies can be observed on a PIC adsorbed Au(111) surface (denoted as PIC/Au(111); Fig. 1f, see inset for the height profile). The strong complexation ability of isocyanide for gold leads to the leaching of gold atoms by PIC during adsorption (Supplementary Section 2). An STM image of a Pd_{ML}/Au(111) surface with PIC adsorption (Fig. 1h, denoted PIC/Pd_{ML}/Au(111)) does not show vacancies, indicating that PIC does not leach Pd atoms.

Time-dependent tip-enhanced Raman spectroscopy (TERS) spectra of PIC/Au(111) and PIC/Pd_{ML}/Au(111) samples are shown in Fig. 2a and c, respectively. The low-frequency vibrations related to the benzene ring appear at similar frequencies for Au and Pd surfaces, that is, 1,000 cm^{-1} (in-plane ring deformation, α_{ring}), 1,165 cm^{-1} (C–H in-plane bending, β_{CH}), 1,192 cm^{-1} (C–NC stretching, ν_{C-NC}) and 1,590 cm^{-1} (C=C stretching, ν_{CC}), consistent with the theoretical spectrum (Fig. 2b and Supplementary Tables 2 and 3). The peaks at 2,190 and 1,995 cm^{-1} correspond to ν_{NC} for the atop and bridge adsorption configurations of PIC on Au on Pd surfaces, respectively (see Supplementary Section 3 for a detailed analysis). For the PIC/Au(111) sample, the ν_{NC} peak can only be observed at the beginning and disappears quickly. After a few minutes of measurement, the spectra contain only the vibrational peaks of the benzene ring, but with a significant broadening of the 1,590 cm^{-1} peak (see Supplementary Fig. 5 for more TERS results obtained under different laser powers). X-ray photoelectron spectroscopy (XPS) results suggest that PIC has been oxidized to phenyl isocyanate on the Au(111) surface (Supplementary Fig. 7). In Fig. 2a, the peak at 1,540 cm^{-1} indicated by the red dashed line can be attributed to the in-plane coupled mode of the phenyl ring and NCO group in phenyl isocyanate (see Supplementary Table 4 and 5 for peak assignments and Section 4 for a discussion), also suggesting the oxidation of PIC. Indeed, despite bulk gold being generally known as a poor catalyst, it can efficiently catalyse various reactions of adsorbed isocyanide under mild conditions[25]. Similar to this study, isocyanide has been found to be oxidized on gold films when exposed to air[26]. In contrast, stable TERS spectra of PIC on Pd_{ML}/Au(111) can be obtained even at a relatively high laser power (Fig. 2c). This indicates that the Pd_{ML}/Au(111) surface is significantly less active than the Au(111) surface for the catalytic oxidation of PIC by oxygen under ambient conditions (see Supplementary Section 4 for a discussion on the catalytic activities of Au and Pd surfaces).

The distinct Raman features of PIC on Au(111) and Pd_{ML}/Au(111) surfaces makes it ideal to detect the electronic and catalytic properties of the heterogeneous bimetallic catalyst surface. For the bare $Pd_{0.8ML}$/Au(111) surface, the sub-ML deposition of Pd leaves

[1]State Key Laboratory of Physical Chemistry of Solid Surfaces, Collaborative Innovation Center of Chemistry for Energy Materials (iChEM), MOE Key Laboratory of Spectrochemical Analysis & Instrumentation, College of Chemistry and Chemical Engineering, Xiamen University, Xiamen 361005, China. [2]Department of Physics, Xiamen University, Xiamen 361005, China. [3]Department of Chemical Engineering, University of South Carolina, Columbia, South Carolina 29208, USA. †These authors contributed equally to this work. *e-mail: bren@xmu.edu.cn

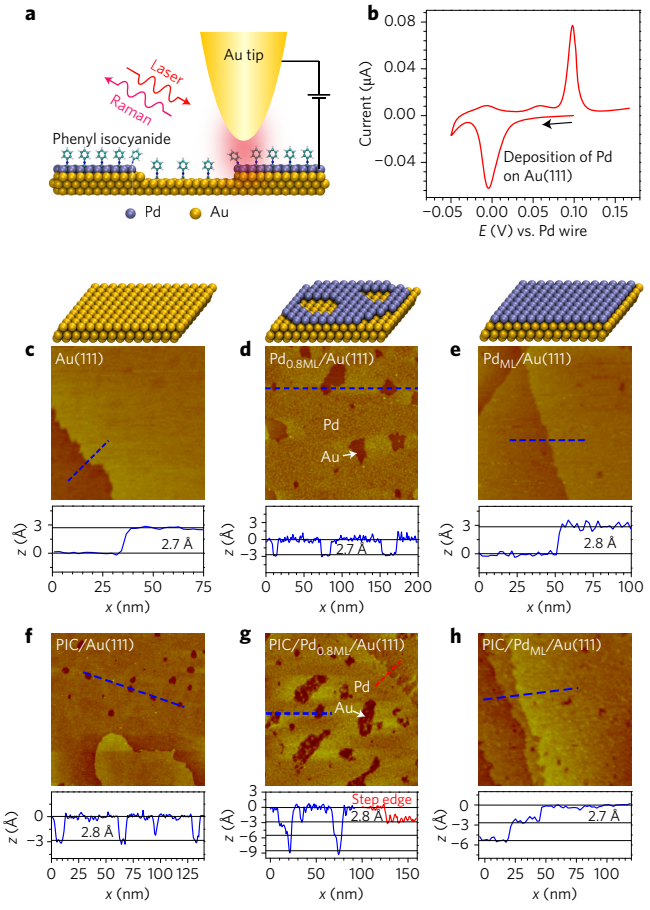

Figure 1 | TERS study of a Pd/Au(111) bimetallic model catalyst. **a**, Schematic of an STM-based TERS configuration using Au tips and Pd/Au(111) substrates with phenyl isocyanide (PIC) on the surface. **b**, CV showing the underpotential deposition of Pd (cathodic peak at −0.005 V) on a Au(111) surface obtained in a solution of 1 mM H_2PdCl_4 and 0.1 M H_2SO_4 at a scan rate of 1 mV s^{-1}. The peak at 0.097 V corresponds to the anodic dissolution of Pd. **c**–**e**, STM images of bare Au(111) (**c**), $Pd_{0.8ML}$/Au(111) (**d**) and Pd_{ML}/Au(111) (**e**) surfaces with corresponding atomic models on top. **f**–**h**, STM images of the surfaces after PIC adsorption for PIC/Au(111) (**f**), PIC/$Pd_{0.8ML}$/Au(111) (**g**) and PIC/Pd_{ML}/Au(111) (**h**) surfaces. Insets below all STM images are height profiles obtained at the dashed lines in the corresponding STM images. All STM images have dimensions of 200 nm × 200 nm and were obtained by Pt-Ir tips.

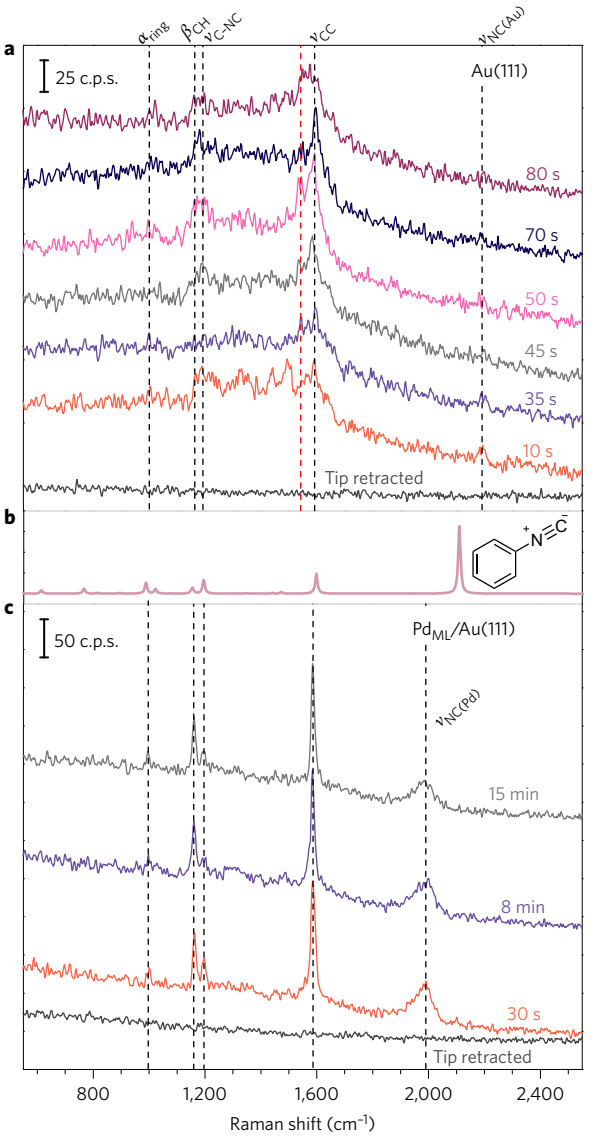

Figure 2 | TERS spectra of PIC. **a**, TERS spectra of PIC adsorbed on a Au(111) surface (0.4 mW, 1 s). **b**, Theoretical Raman spectrum of free PIC molecule. Inset: chemical structure of PIC. **c**, TERS spectra of PIC adsorbed on a Pd_{ML}/Au(111) surface (1.2 mW, 1 s).

some gold holes with monoatomic depth (Fig. 1d). In comparison, the depth of the gold holes increases from monoatomic to two or three atoms high after the adsorption of PIC on the $Pd_{0.8ML}$/Au(111) surface, denoted as PIC/$Pd_{0.8ML}$/Au(111) (Fig. 1g). This observation is similar to that on Au(111) surface, where the increase in the depth of gold holes can be attributed to the leaching of gold atoms by PIC (PIC adopts a similar vertical configuration on Au and Pd surfaces, Supplementary Fig. 2). Another STM image (Fig. 3a) of the PIC/$Pd_{0.8ML}$/Au(111) sample shows a region with a gold hole surrounded by Pd ML. Figure 3b plots the line-trace TERS spectra acquired along the line marked in Fig. 3a, with the tip moving across Pd_{ML}–Au hole–Pd_{ML} regions (for more data sets see Fig. 3c and Supplementary Fig. 9). The TERS spectra clearly evolve from the Pd_{ML} to the Au hole and back to the Pd_{ML} region (Fig. 3b,c), which complements the STM topography but provides rich chemical information. The oxidation of PIC on the Au hole region is evidenced by the appearance of the 2,245 cm^{-1} peak (Supplementary Fig. 5), assigned to the stretching vibration of the N=C=O bond (ν_{NCO}).

The variation of the TERS intensity can be seen as a colour-coded map in Fig. 3c, offering a clear chemical contrast between the Pd_{ML} and Au hole surfaces. The intensities of the three main peaks (1,165, 1,590 and 1,995 cm^{-1}) are plotted as a function of tip position in Fig. 3d (see Supplementary Section 6 for the procedure for intensity analysis). The decrease in the intensities of the 1,165 and 1,590 cm^{-1} bands in the Au hole region is mainly ascribed to a lower PIC coverage on the Au than on the Pd surface (Supplementary Section 7). The intensity of the 1,995 cm^{-1} peak should decrease to zero in the Au hole region. The ν_{NC} of PIC on the Au surface should appear at ~2,190 cm^{-1}. However, this peak was not observed due to the oxidation of PIC. The intensity profiles of all three bands match well with the height profile (Fig. 3d), indicating that the site-specific chemical properties of the $Pd_{0.8ML}$/Au(111) bimetallic surface have been spatially resolved.

Another striking feature of Fig. 3d is the enhanced TERS intensities of all three bands at the step edges, which may result from either a higher local coverage or a stronger electromagnetic field at the step edge. There would be not much difference for the

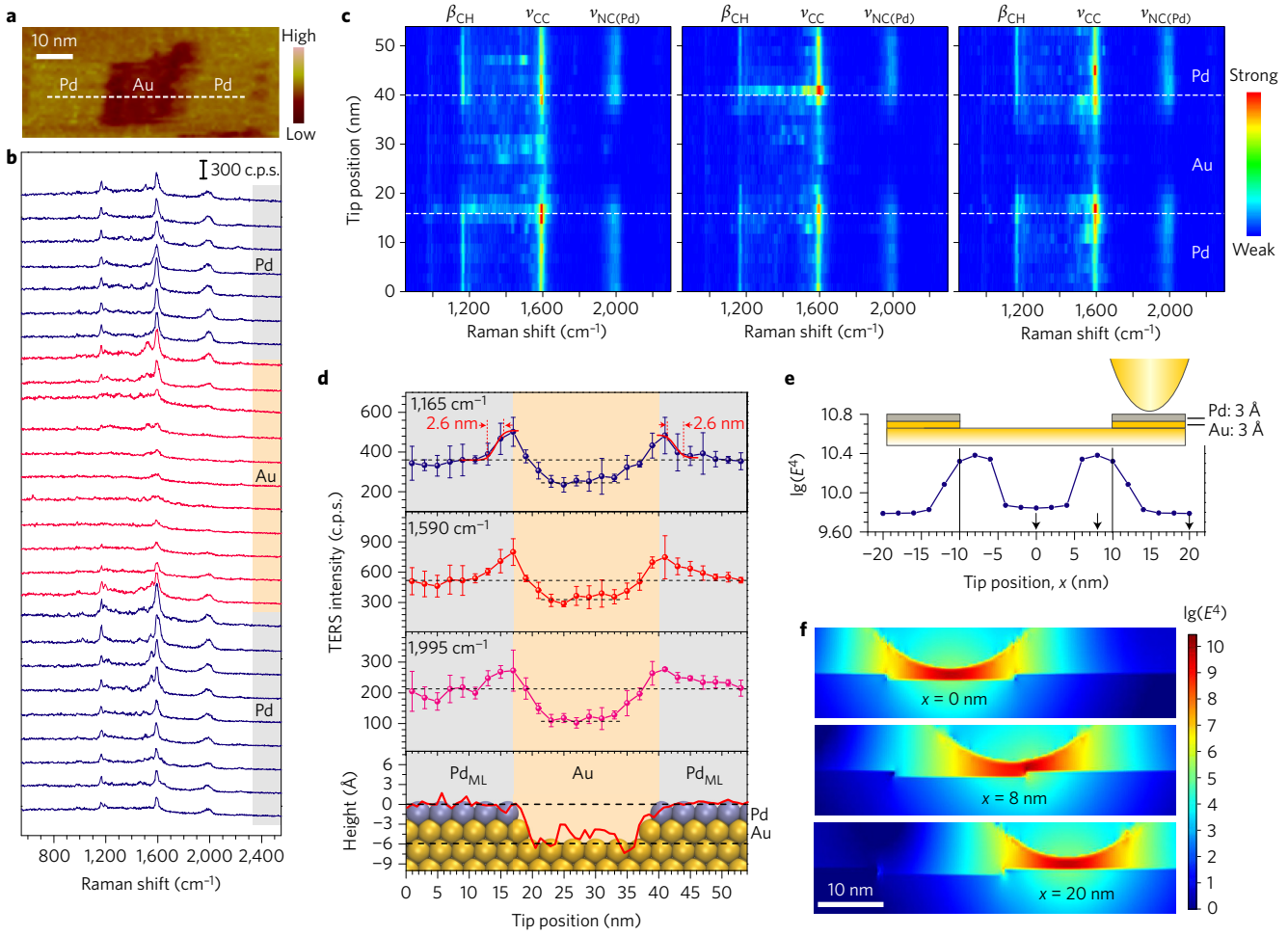

Figure 3 | TERS images of a Pd/Au(111) bimetallic surface. a, STM image of the $Pd_{0.8ML}$/Au(111) surface with adsorbed PIC, obtained using a gold tip, showing a gold hole in the centre. **b**, Line-trace TERS spectra acquired along the dashed line in **a**. **c**, Colour-coded intensity map of three line-trace TERS images taken in succession. The background is subtracted for a better view of the variation in Raman intensities. **d**, Top three panels: plots of intensities of the three main TERS peaks (1,165, 1,590 and 1,995 cm^{-1}) with the tip position. Error bars indicate standard deviation for the three measurements. Bottom panel: topographic height profile of the surface along the dashed line in **a**, superimposed with the atomic model of the surface atoms. The size of atoms is to scale on the *y* axis but not to scale on the *x* axis. Purple, Pd; yellow, Au. One layer of gold is leached to form two-atom-high steps (~6 Å). The adsorbed PIC molecules on the surface are not included in the model. **e**, Calculated TERS enhancement factor when an Au tip is located at different positions of a Pd–Au–Pd surface (top inset: substrate model for calculation). The effect of electron surface scattering on the optical response of the Pd atomic layer has been considered in calculations (Supplementary Section 8). Arrows in **e** indicate tip positions at $x = 0$, 8, 20 nm. **f**, Calculated TERS enhancement distribution at the *x*–*z* plane when the tip is positioned on Au ($x = 0$ nm), the step edge ($x = 8$ nm) and Pd ($x = 20$ nm) surface.

molecular coverage at the step edge and terrace, because the coverage of PIC on the Pd_{ML}/Au(111) surface is about a full monolayer (Supplementary Section 7). We simulated the electromagnetic field at the step edge using a finite-difference time-domain method. The results suggest a stronger electromagnetic field at the step edges than on the Au and Pd_{ML} terraces (Fig. 3e,f), qualitatively explaining the experimental results. This enhancement can be understood by the lightning-rod effect (non-resonant), because of the decrease in the effective curvature radius at the step edge compared with the terrace and the possible plasmonic effect (resonant) due to the accumulation of surface charges at the step edge. This is similar to the observation that a 2-nm-high step edge could produce a stronger TERS intensity than flat surface sites[27] and the theoretical prediction of a stronger localization of electromagnetic fields at atomic step features[28]. The spatial resolution is estimated to be ~3 nm within a 10–90% contrast (Fig. 3d) or a full-width at half-maximum (FWHM) analysis (Supplementary Fig. 13).

It would be interesting to see if we can distinguish the electronic and catalytic properties of the atoms at different surface sites. Figure 4a presents an STM image (height profile in Fig. 4b) from another Pd–Au–Pd region of the PIC/$Pd_{0.8ML}$/Au(111) sample. The line-scan TERS spectra show only one peak at ~1,995 cm^{-1} at the Pd terrace, and another lower frequency peak at ~1,933 cm^{-1} appears when the tip approaches Pd edges (Fig. 4c,d; for more data see Supplementary Fig. 14). The 1,933 cm^{-1} peak has a much narrower FWHM (~35 cm^{-1}) than the 1,995 cm^{-1} peak (~60 cm^{-1}), indicating a distinct molecular adsorption state. We attribute this peak to a rise from PIC adsorbed at the Pd step edges.

Density functional theory (DFT) calculations were performed to elucidate the local electronic structure of the Pd terrace and step edges, and to understand the different peak frequencies and reaction activities for the PIC molecule at these two sites (analysis of the electronic structure of adjacent Au atoms can be found in Supplementary Fig. 15). Figure 4e and f are the simulation models for the Pd terrace and step edge (using an island-like Pd overlayer), respectively. Figure 4g shows the projected electronic density of states (DOS) of *d*-bands on clean Pd atoms at different surface sites. The inner two Pd atoms (numbered 1 and 2 in Fig. 4f) have a similar *d*-band profile to the terrace Pd atom (solid blue line in Fig. 4g), while the adjacent atom of step edge (number 3 in

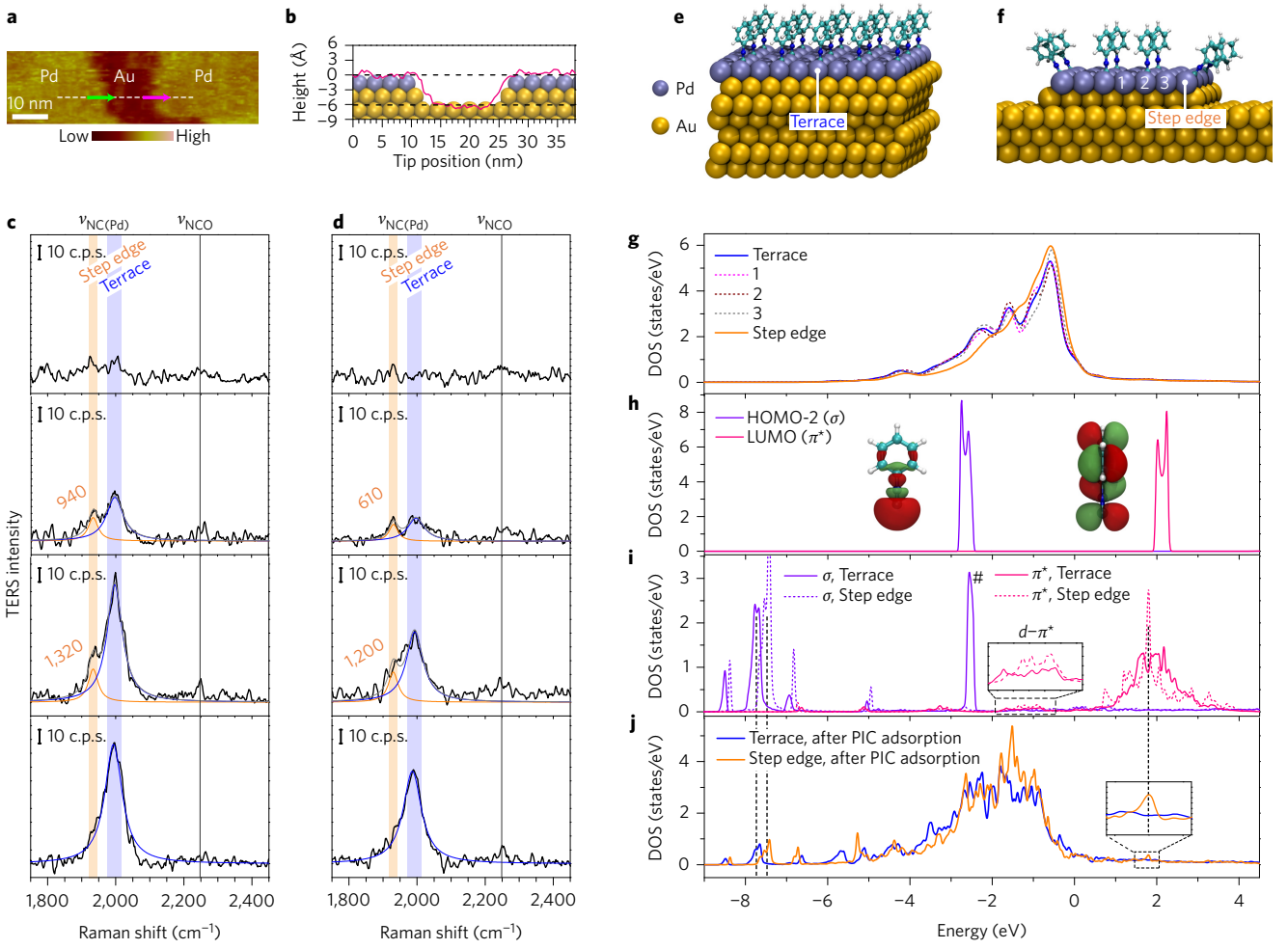

Figure 4 | Electronic properties of Pd step edges. a, STM image of a PIC/$Pd_{0.8ML}$/Au(111) surface obtained using a gold tip. **b**, Height profile along the dashed line in **a**, superimposed with the atomic model of the surface atoms (the size of atoms is to scale on the *y* axis but not to scale on the *x* axis). **c**, Line-scan TERS spectra (from bottom to top) across a Pd terrace–Pd step edge–Au terrace region (indicated by green arrow in **a**). **d**, Line-scan TERS spectra (from top to bottom) across a Au terrace–Pd step edge–Pd terrace region (indicated by pink arrow in **a**). The spectra in **c** and **d** are smoothed, background-subtracted and fitted by a Lorentz function. The fitted area of the 1,933 cm^{-1} peak is indicated beside the peak in light red. **e**,**f**, Atomic models for simulation of the electronic structure of the Pd terrace (**e**) and Pd step edge (**f**) on a Au(111) surface. **g**, Calculated projected electronic DOS of clean Pd atoms at different surface sites (indicated in **e** and **f**). **h**, Projected DOS of HOMO-2 and LUMO of the NC bond of the PIC molecule in vacuum (inset: isosurface of the corresponding molecular orbital wavefunction). **i**, Projected DOS on molecular orbitals when PIC is adsorbed on Pd terrace and step edge sites. The peak marked with # originates from molecular-level crossing when performing molecular orbital projection (Supplementary Section 3.5). **j**, Projected DOS of terrace and step edge Pd atoms after PIC adsorption. Vertical dashed lines in **i** and **j** indicate matching peaks of projected DOS on molecular orbitals (**i**) and Pd atoms (**j**), as discussed in the main text.

Fig. 4f) has a higher peak at the top of the *d*-band. The projected DOS of the step-edge Pd atom has a global shift to higher energy and a narrowing of the *d*-band (solid orange line in Fig. 4g), as a result of its unsaturated coordination and thus the decrease in inter-atom coupling[29].

Figure 4h presents the energy levels of the σ lone electron pair molecular orbital (HOMO-2) and unoccupied π^* molecular orbital (LUMO) of the PIC molecule in vacuum; these are the dominant frontier orbitals interacting with the metal substrate. After interaction of PIC with Pd, the σ orbital of PIC hybridizes with the *d* states of the Pd atom and shifts to lower energies at ~−8.0 eV (Fig. 4i), and the projected DOS of the Pd atoms show matching peaks (Fig. 4j), confirming the σ–*d* interaction. The σ orbital of PIC adsorbed at the step edge (Fig. 4i, dashed purple line) is at higher energies than that at the terrace (Fig. 4i, solid purple line), indicating a weaker σ–*d* interaction at the step edge[30]. In comparison to the terrace case (Fig. 4i, solid pink line), a stronger back donation of the *d* electrons of the Pd atom to the π^* orbital of the PIC molecules at the step edge is evidenced by (1) the more significant splitting and broadening of the π^* orbital (Fig. 4i, dashed pink line); (2) stronger d–π^* interacting peaks at ~−1.0 eV (Fig. 4i inset, dashed pink line) and (3) the appearance of resonating peaks at ~1.8 eV (Fig. 4j inset, solid orange line), which are absent for terrace adsorption. Taken together, the upshift of the electronic *d*-band profile at the step edge decreases the σ–*d* interaction but enhances the d–π^* back-donation, which weakens the NC bond strength.

Calculations of vibrational frequencies support these findings. The calculated ν_{NC} frequencies of PIC adsorbed at terrace and step edge are 1,965 and 1,905 cm^{-1}, respectively (Supplementary Table 1 and 2). The redshift of 60 cm^{-1} from terrace to step edge is in agreement with the experimental results (Fig. 4c,d). The lower frequency peak indicates a weaker NC bond of PIC adsorbed at the step edge than that at terraces. Because PIC has the same bridge adsorption configuration and comparable binding affinity at the Pd step edge and terrace, the weakened NC bond at the step edge becomes more labile for oxidation. Indeed, from the

results in Fig. 4c,d and Supplementary Fig. 14, the ν_{NCO} peak at 2,250 cm^{-1} can generally be observed at Pd step edges but not at terraces (similar results for the in-plane coupled mode are presented in Supplementary Fig. 6). These results suggest a higher activity for PIC oxidation at the Pd step edge than that at the terrace. The spatially resolved TERS provides unambiguous evidence regarding the unique electronic and catalytic properties of the Pd step edge.

In summary, we have demonstrated that the site-specific electronic and catalytic properties of a Pd/Au(111) bimetallic surface can be spatially resolved at 3 nm resolution in real space. The ability to spatially distinguish the molecular vibrational features of molecules adsorbed at different surface sites will allow a more detailed understanding of heterogeneous catalysis. TERS is ideally suited to the study of defects, step edges and perimetrical interfaces of various catalytic materials, which, while often representing a minority of surface sites, can play a crucial role in determining catalytic performance. It is expected that the application of TERS will be useful for catalysis studies at atomic and molecular levels, eventually leading to an improved nanoscale design of catalysts.

Methods

Methods and any associated references are available in the online version of the paper.

Received 5 July 2016; accepted 7 October 2016;
published online 21 November 2016

References

1. Buurmans, I. L. C. & Weckhuysen, B. M. Heterogeneities of individual catalyst particles in space and time as monitored by spectroscopy. *Nat. Chem.* **4,** 873–886 (2012).
2. Ding, K. *et al.* Identification of active sites in CO oxidation and water-gas shift over supported Pt catalysts. *Science* **350,** 189–192 (2015).
3. Chen, G. *et al.* Interfacial effects in iron-nickel hydroxide-platinum nanoparticles enhance catalytic oxidation. *Science* **344,** 495–499 (2014).
4. Stöckle, R. M., Suh, Y. D., Deckert, V. & Zenobi, R. Nanoscale chemical analysis by tip-enhanced Raman spectroscopy. *Chem. Phys. Lett.* **318,** 131–136 (2000).
5. Anderson, M. S. Locally enhanced Raman spectroscopy with an atomic force microscope. *Appl. Phys. Lett* **76,** 3130–3132 (2000).
6. Hayazawa, N., Inouye, Y., Sekkat, Z. & Kawata, S. Metallized tip amplification of near-field Raman scattering. *Opt. Commun.* **183,** 333–336 (2000).
7. Pettinger, B., Schambach, P., Villagómez, C. J. & Scott, N. Tip-enhanced Raman spectroscopy: near-fields acting on a few molecules. *Annu. Rev. Phys. Chem.* **63,** 379–399 (2012).
8. Berweger, S. *et al.* Optical nanocrystallography with tip-enhanced phonon Raman spectroscopy. *Nat. Nanotech.* **4,** 496–499 (2009).
9. Liu, Z. *et al.* Revealing the molecular structure of single-molecule junctions in different conductance states by fishing-mode tip-enhanced Raman spectroscopy. *Nat. Commun.* **2,** 305 (2011).
10. Yano, T. A. *et al.* Tip-enhanced nano-Raman analytical imaging of locally induced strain distribution in carbon nanotubes. *Nat. Commun.* **4,** 2592 (2013).
11. Zhang, R. *et al.* Chemical mapping of a single molecule by plasmon-enhanced Raman scattering. *Nature* **498,** 82–86 (2013).
12. Jiang, S. *et al.* Distinguishing adjacent molecules on a surface using plasmon-enhanced Raman scattering. *Nat. Nanotech.* **10,** 865–869 (2015).
13. Zeng, Z.-C. *et al.* Electrochemical tip-enhanced Raman spectroscopy. *J. Am. Chem. Soc.* **137,** 11928–11931 (2015).
14. Kurouski, D., Mattei, M. & Van Duyne, R. P. Probing redox reactions at the nanoscale with electrochemical tip-enhanced Raman spectroscopy. *Nano Lett.* **15,** 7956–7962 (2015).
15. van Schrojenstein Lantman, E. M., Deckert-Gaudig, T., Mank, A. J. G., Deckert, V. & Weckhuysen, B. M. Catalytic processes monitored at the nanoscale with tip-enhanced Raman spectroscopy. *Nat. Nanotech.* **7,** 583–586 (2012).
16. Sun, M., Zhang, Z., Zheng, H. & Xu, H. *In-situ* plasmon-driven chemical reactions revealed by high vacuum tip-enhanced Raman spectroscopy. *Sci. Rep.* **2,** 647 (2012).
17. Kumar, N., Stephanidis, B., Zenobi, R., Wain, A. J. & Roy, D. Nanoscale mapping of catalytic activity using tip-enhanced Raman spectroscopy. *Nanoscale* **7,** 7133–7137 (2015).
18. Domke, K. F. & Pettinger, B. *In situ* discrimination between axially complexed and ligand-free Co porphyrin on Au(111) with tip-enhanced Raman spectroscopy. *ChemPhysChem* **10,** 1794–1798 (2009).
19. Hartman, T., Wondergem, C. S., Kumar, N., van den Berg, A. & Weckhuysen, B. M. Surface- and tip-enhanced Raman spectroscopy in catalysis. *J. Phys. Chem. Lett.* **7,** 1570–1584 (2016).
20. Chen, M., Kumar, D., Yi, C.-W. & Goodman, D. W. The promotional effect of gold in catalysis by palladium-gold. *Science* **310,** 291–293 (2005).
21. Zhang, H., Watanabe, T., Okumura, M., Haruta, M. & Toshima, N. Catalytically highly active top gold atom on palladium nanocluster. *Nat. Mater.* **11,** 49–52 (2012).
22. Nenajdenko, V. G. (ed.) *Isocyanide Chemistry: Applications in Synthesis and Material Science* (Wiley-VCH, 2012).
23. Hu, J., Tanabe, M., Sato, J., Uosaki, K. & Ikeda, K. Effects of atomic geometry and electronic structure of platinum surfaces on molecular adsorbates studied by gap-mode SERS. *J. Am. Chem. Soc.* **136,** 10299–10307 (2014).
24. Hu, J., Hoshi, N., Uosaki, K. & Ikeda, K. Vibrational spectroscopic observation of atomic-scale local surface sites using site-selective signal enhancement. *Nano Lett.* **15,** 7982–7986 (2015).
25. Lazar, M. & Angelici, R. J. Gold metal-catalyzed reactions of isocyanides with primary amines and oxygen: analogies with reactions of isocyanides in transition metal complexes. *J. Am. Chem. Soc.* **128,** 10613–10620 (2006).
26. Stapleton, J. J. *et al.* Self-assembly, characterization, and chemical stability of isocyanide-bound molecular wire monolayers on gold and palladium surfaces. *Langmuir* **21,** 11061–11070 (2005).
27. Zhang, W. H. *et al.* Nanoscale roughness on metal surfaces can increase tip-enhanced Raman scattering by an order of magnitude. *Nano Lett.* **7,** 1401–1405 (2007).
28. Barbry, M. *et al.* Atomistic near-field nanoplasmonics: reaching atomic-scale resolution in nanooptics. *Nano Lett.* **15,** 3410–3419 (2015).
29. Hammer, B. & Nørskov, J. K. Theoretical surface science and catalysis—calculations and concepts. *Adv. Catal.* **45,** 71–129 (2000).
30. Kresse, G., Gil, A. & Sautet, P. Significance of single-electron energies for the description of CO on Pt(111). *Phys. Rev. B* **68,** 073401 (2003).

Acknowledgements

The authors acknowledge support from MOST (2016YFA0200601, 2013CB933703 and 2011YQ03012400), NSFC (21633005, 21227004, 21321062 and J1310024) and MOE (IRT13036). The authors thank J.M. Feliu, N. Zheng, D.-Y. Wu, M. Zhang, X.-G. Zhang and A. Terfort for discussions, S. Mo for assistance with ICP-MS measurements and Y. Zheng for help with XPS measurements. The authors acknowledge the National Supercomputer Center in Guangzhou for Tianhe-2 CPU time and assistance. C.T.W. acknowledges support from the PCOSS fellowship programme.

Author contributions

B.R. supervised the project. J.-H.Z. and B.R. conceived the ideas. J.-H.Z., X.W. and H.-S.S performed the experiments. X.J. performed electronic structure and vibrational frequency calculations. L.M. and Z.-L.Y. performed electromagnetic field simulations. C.T.W. helped with experiments and analysis. All authors contributed to data interpretation and writing of the manuscript.

Additional information

Supplementary information is available in the online version of the paper. Reprints and permissions information is available online at www.nature.com/reprints. Correspondence and requests for materials should be addressed to B.R.

Competing financial interests

The authors declare no competing financial interests.

Methods

Pd was electrodeposited onto Au(111) surfaces by cyclic voltammogram (CV) at a scan rate of 1 mV s^{-1}, in a solution of 1 mM H_2PdCl_4 and 0.1 M H_2SO_4. PIC was allowed to adsorb and form a self-assembled monolayer on the Au(111) and Pd/Au (111) surfaces by immersing the substrates in a 20 μM ethanoic solution of PIC for 30 min. Electrochemically etched gold tips were used for TERS measurements. In a TERS line-trace imaging experiment, the tip was scanned at a velocity of 2 nm s^{-1} and TERS spectra were acquired simultaneously in an integration time of 1 s (1 spectrum per second; that is, one spectrum is acquired for every 2 nm of surface distance). A laser power of 0.7 mW was used in all TERS imaging experiments. All the STM images and TERS spectra were acquired under a tunnelling condition of 200 pA and 600 mV. Note that the line-trace imaging experiments were performed after a few hours of TERS measurements (continuous laser illumination) to maximally decrease the drift of the system to ~2 nm min^{-1}. The three-dimensional finite-difference time-domain (3D-FDTD) method was used to calculate the TERS enhancement factor. DFT calculations were performed with the Perdew–Burke–Ernzerhof functional and projector augmented-wave method, as implemented in Quantum ESPRESSO package[31].

References

31. Giannozzi, P. *et al.* QUANTUM ESPRESSO: a modular and open-source software project for quantum simulations of materials. *J. Phys. Condens. Matter* **21,** 395502 (2009).